Landau-Ginzburg theory of charge density wave formation accompanying lattice and electronic long-range ordering

Anna N. Morozovska [1,*] Eugene A. Eliseev [2] Venkatraman Gopalan [3,†] and Long-Qing Chen [3,‡]

[1]*Institute of Physics, National Academy of Sciences of Ukraine, 41, pr. Nauki, 03028 Kyiv, Ukraine*

[2]*Institute for Problems of Materials Science, National Academy of Sciences of Ukraine, 3, Krjijanovskogo, 03142 Kyiv, Ukraine*

[3]*Department of Materials Science and Engineering, Pennsylvania State University, University Park, Pennsylvania 16802, USA*

(Received 21 December 2022; revised 15 March 2023; accepted 25 April 2023; published 8 May 2023)

We propose an analytical Landau-Ginzburg (LG) theory of the charge density waves coupled with lattice and electronic long-range order parameters. Examples of long-range order include the electronic wave function of superconducting Cooper pairs, structural distortions, electric polarization, and magnetization. We formulate the LG free energy density as a power expansion with respect to the charge density and other long-range order parameters as well as their spatial gradients and biquadratic coupling terms. We introduced a biquadratic coupling between the charge density gradient and long-range order parameters as well as nonlinear higher gradients of the long-range order parameters. The biquadratic gradient coupling is critical to the appearance of different spatially modulated phases in charge-ordered ferroics and high-temperature superconductors. We derived the thermodynamic conditions for the stability of the spatially modulated phases, which are the intertwined spatial waves of charge density and lattice/electronic long-range order. The analytical expressions for the energies of different phases, corresponding order parameters, charge density waves amplitudes, and modulation periods obtained in this paper can be employed to guide the comprehensive physical explanation, deconvolution, and Bayesian analysis of experimental data on quantum materials ranging from charge-ordered ferroics to high-temperature superconductors.

DOI: 10.1103/PhysRevB.107.174104

I. INTRODUCTION

The formation of charge density waves may lead to anomalies in the electrophysical properties of bulk and two-dimensional (2D) transition metal dichalcogenides [1–3]; high-temperature superconducting cuprates [4,5]; resistive switching materials [6,7]; ferroics and multiferroics [8,9] exhibiting long-range structural, magnetic [10], antiferrodistortive, and/or polar [11,12] orders; and electric charge ordering. In many cases, superconductivity; spin, structural, orbital, or polar ordering; and charge density waves are competing orders [13], which can coexist and often become coupled or intertwined [14–16], manifesting a complex interplay arising from strong intraorder correlations. For instance, Beaud *et al.* [17] revealed that the relaxation of orbital ordering (pseudo-Jahn-Teller mode) and charge ordering are coupled in a perovskite manganite. Hamidian *et al.* [18] demonstrated the existence of spatial modulation of the density of Cooper pairs in a superconductor naturally coupled with phonon modes.

Incommensurate charge density waves, which are periodic spatial modulations of the electronic density uncorrelated with the lattice period, are ubiquitous in multiferroics [11] and superconducting cuprates [5]. Nie *et al.* [19] proposed an effective field theory of a layered system with incommensurate spin- and/or charge-density wave orders in hole-doped cuprates. Wang *et al.* [20] also analyzed the interplay between a uniform superconducting and a pair-density-wave order parameter in the neighborhood of a vortex and, using a phenomenological nonlinear sigma model, revealed that the intertwining of the two superconducting orders leads to a charge density modulation with the same periodicity as the pair-density wave. Using the Landau-Ginzburg-Wilson theory of competing orders, Yu and Kivelson [21] demonstrated the generic occurrence of a fragile superconducting phase at low temperatures in the presence of weak charge-density-wave disorder and proposed an explanation of the discovered resilient superconducting phase at high fields in underdoped $YBa_2Cu_3O_{6+x}$.

In this regard, ferroics and high-temperature superconductors in the presence of charge density waves are very sensitive to the spatial gradients of long-range order parameters [22,23]. Among many theoretical approaches (see, e.g., Ref. [24]), the Landau-Ginzburg (LG)-type models [1,2,5,13,17,18,25], which account for the spatial gradients of order parameters, have played a central role in understanding the formation of incommensurate charge density waves and their dynamics and interaction with lattice and electronic long-range order parameters, such as (anti)ferromagnetic, (anti)ferroelectric, (anti)ferrodistortive, and/or superconducting orders. In the general case, LG models that include implicit expressions for depolarization (demagnetization) fields are self-consistent. Also, LG models allow analytical

*anna.n.morozovska@gmail.com
†vgopalan@psu.edu
‡lqc3@psu.edu

descriptions of complex coupled problems, including phase diagrams and incommensurate modulation periods. Analytical LG models significantly simplify physical explanation. They can provide a comprehensive deconvolution of experimental data and are suitable for their Bayesian analysis [26,27] and complex machine learning.

In this paper, we aim to propose an analytical LG theory of the coupled charge density waves and lattice/electronic long-range ordering in ferroics and high-temperature superconductors. We formulate the LG free energy power expansion with respect to the charge density and other long-range order parameter(s), e.g., a wave function of superconducting Cooper pairs, structural distortion, electric polarization, magnetization, their spatial gradients, and biquadratic coupling terms [1,2,5,13]. The structure of gradient terms in the free energy functional used in this paper is different from earlier LG models [1,2,5,13]. We introduced a biquadratic coupling between the charge density gradient and lattice/electronic long-range order and nonlinear higher gradients of the long-range orders. Our primary interests are the determination of the appearance and stability conditions of the spatially modulated phases [28], which are the coupled spatial waves of charge density and spontaneous (e.g., superconductive, polar, or magnetic) long-range order. The gradient terms introduced in this paper are critical to the appearance of the spatially modulated phases.

We formulate the LG model in Sec. II. The phase diagrams, including the analytical expressions for stability conditions, amplitudes, and modulation periods for the spatially modulated phases, are presented in Secs. III and IV. Section V provides the conclusions.

II. PROBLEM FORMULATION

Following McMillan [1,2] and Wandel *et al.* [5], we consider complex order parameters to be vectorial and/or scalar, and use $\boldsymbol{\psi}_{\mathrm{C}}$ and $\boldsymbol{\psi}_{\mathrm{S}}$ to denote the charge density (C) and spontaneous (S) long-range orders, respectively. The primary purpose of this paper is to analyze the spatially modulated phases in a system described by the LG free energy functional of the $\boldsymbol{\psi}_{\mathrm{C}}$ and $\boldsymbol{\psi}_{\mathrm{S}}$ orders. These include the spatial waves of the charge density (CW), which is a $\boldsymbol{\psi}_{\mathrm{C}}$ spatial modulation; spatial waves of the spontaneous long-range order (SW), which is a $\boldsymbol{\psi}_{\mathrm{S}}$ spatial modulation; and intertwined spatial waves of charge density and spontaneous long-range order (SCW), which are coupled spatial modulation of both $\boldsymbol{\psi}_{\mathrm{C}}$ and $\boldsymbol{\psi}_{\mathrm{S}}$. The total free energy of a system is then expressed as a functional of $\boldsymbol{\psi}_{\mathrm{C}}$ and $\boldsymbol{\psi}_{\mathrm{S}}$:

$$F[\boldsymbol{\psi}_{\mathrm{C}},\ \boldsymbol{\psi}_{\mathrm{S}}] = \int \left(f_{\mathrm{int}}[\boldsymbol{\psi}_{\mathrm{C}}, \boldsymbol{\psi}_{\mathrm{S}}] + f_{\mathrm{C0}}[\boldsymbol{\psi}_{\mathrm{C}}] + f_{\mathrm{S0}}[\boldsymbol{\psi}_{\mathrm{S}}]\right) d^3\vec{r}. \tag{1a}$$

Following She *et al.* [13], we assume that the interaction energy $f_{\mathrm{int}}[\boldsymbol{\psi}_{\mathrm{C}}, \boldsymbol{\psi}_{\mathrm{S}}]$ has the simplest form of biquadratic coupling of the order parameters $f_{\mathrm{int}} \sim \eta_{ij}|\psi_{\mathrm{C}i}|^2|\psi_{\mathrm{S}j}|^2$ introduced by Haun *et al.* [29], Houchmanzadeh *et al.* [30], and Balashova and Tagantsev [31]. Since the interactions between the order parameter gradients are very important, we also add the biquadratic gradient-coupling terms to $f_{\mathrm{int}}[\boldsymbol{\psi}_{\mathrm{C}}, \boldsymbol{\psi}_{\mathrm{S}}]$, which acquires the form:

$$\begin{aligned} f_{\mathrm{int}}[\boldsymbol{\psi}_{\mathrm{C}}, \boldsymbol{\psi}_{\mathrm{S}}] = {} & \eta_{ij}|\psi_{\mathrm{C}i}|^2|\psi_{\mathrm{S}j}|^2 \\ & + \xi_{ijk}\left(|\psi_{\mathrm{S}i}|^2\left|\frac{\partial\psi_{\mathrm{C}j}}{\partial x_k}\right|^2 + |\psi_{\mathrm{C}i}|^2\left|\frac{\partial\psi_{\mathrm{S}j}}{\partial x_k}\right|^2\right) \\ & + \chi_{ijkl}\left|\frac{\partial\psi_{\mathrm{C}i}}{\partial x_j}\right|^2\left|\frac{\partial\psi_{\mathrm{S}k}}{\partial x_l}\right|^2. \end{aligned} \tag{1b}$$

Hereinafter, the summation takes place over all repeated subscripts, $i\ i,\ j,\ k = 1, 2,$ or 3 for vectorial order parameter(s).

Note that the flexo-type bilinear gradient-coupling terms, such as $\gamma_{ijk}(\psi_{\mathrm{C}i}\frac{\partial}{\partial x_j}\psi_{\mathrm{S}k} - \psi_{\mathrm{S}k}\frac{\partial}{\partial x_j}\psi_{\mathrm{C}i})$, can exist for observable real quantities (see, e.g., Ref. [11] and Table I therein). The presence of a nonzero flexo-coupling tensor γ_{ijk} strongly depends on the material spatial symmetry and tensorial and time-reversal properties of the order parameters [11]. Since the absolute value $|\psi_{\mathrm{C}i}\frac{\partial}{\partial x_j}\psi_{\mathrm{S}k} - \psi_{\mathrm{S}k}\frac{\partial}{\partial x_j}\psi_{\mathrm{C}i}|$ is incompatible with minimization over $\boldsymbol{\psi}^*_{\mathrm{C}}$ and $\boldsymbol{\psi}^*_{\mathrm{S}}$, one should consider the complex form of the flexo-type bilinear gradient-coupling, e.g., $\frac{\gamma_{ijk}}{2}[(\psi^*_{\mathrm{C}i}\frac{\partial}{\partial x_j}\psi_{\mathrm{S}k} - \psi_{\mathrm{S}k}\frac{\partial}{\partial x_j}\psi^*_{\mathrm{C}i}) + (\psi_{\mathrm{C}i}\frac{\partial}{\partial x_j}\psi^*_{\mathrm{S}k} - \psi^*_{\mathrm{S}k}\frac{\partial}{\partial x_j}\psi_{\mathrm{C}i})]$, where the tensor γ_{ijk} is very sensitive to the symmetry and tensorial and time-reversal properties of $\boldsymbol{\psi}_{\mathrm{C}}$ and $\boldsymbol{\psi}_{\mathrm{S}}$. For instance, in a one-dimensional (1D) approximation for scalar functions ψ_{C} and ψ_{S}, the term $\frac{\gamma}{2}[(\psi^*_{\mathrm{C}}\frac{\partial}{\partial x}\psi_{\mathrm{S}} - \psi_{\mathrm{S}}\frac{\partial}{\partial x}\psi^*_{\mathrm{C}}) + (\psi_{\mathrm{C}}\frac{\partial}{\partial x}\psi^*_{\mathrm{S}} - \psi^*_{\mathrm{S}}\frac{\partial}{\partial x}\psi_{\mathrm{C}})]$ changes its sign under the x-inversion operation $x \to -x$. Since the free energy of the parent (disordered) phase should be invariant with respect to the spatial inversion, the flexo-coupling coefficient $\gamma = 0$. The coefficient γ can be nonzero when, e.g., ψ_{C} is a scalar and ψ_{S} is an x component of a polar vector, ψ_{C} is a scalar and ψ_{S} is a pseudoscalar, or ψ_{C} is an x component of an axial vector and ψ_{S} is an x component of a polar vector. These specific cases will be considered elsewhere; below, we consider only the biquadratic gradient-coupling terms in f_{int}, which are nonzero for arbitrary symmetry and tensorial and time-reversal properties of $\boldsymbol{\psi}_{\mathrm{C}}$ and $\boldsymbol{\psi}_{\mathrm{S}}$.

As suggested by She *et al.* [13], the contributions f_{CO} and f_{SO} have the following form:

$$\begin{aligned} f_{\mathrm{CO}}[\boldsymbol{\psi}_{\mathrm{C}}] = {} & a_{\mathrm{C}i}|\psi_{\mathrm{C}i}|^2 + b_{\mathrm{C}ij}|\psi_{\mathrm{C}i}|^2|\psi_{\mathrm{C}j}|^2 + g_{\mathrm{C}ij}\left|\frac{\partial\psi_{\mathrm{C}i}}{\partial x_j}\right|^2 \\ & + \left(w_{\mathrm{C}ij}\left|\frac{\partial\psi_{\mathrm{C}i}}{\partial x_j}\right|^2 + v_{\mathrm{C}ij}\left|\frac{\partial^2\psi_{\mathrm{C}i}}{\partial x_j^2}\right|^2\right)|\psi_{\mathrm{C}i}|^2, \end{aligned} \tag{1c}$$

$$\begin{aligned} f_{\mathrm{SO}}[\boldsymbol{\psi}_{\mathrm{S}}] = {} & a_{\mathrm{S}i}|\psi_{\mathrm{S}i}|^2 + b_{\mathrm{S}ij}|\psi_{\mathrm{S}i}|^2\left|\psi_{\mathrm{S}j}\right|^2 + g_{\mathrm{S}ij}\left|\frac{\partial\psi_{\mathrm{S}i}}{\partial x_j}\right|^2 \\ & + \left(w_{\mathrm{S}ij}\left|\frac{\partial\psi_{\mathrm{S}i}}{\partial x_j}\right|^2 + v_{\mathrm{S}ij}\left|\frac{\partial^2\psi_{\mathrm{S}i}}{\partial x_j^2}\right|^2\right)|\psi_{\mathrm{S}i}|^2. \end{aligned} \tag{1d}$$

Due to the presence of biquadratic gradient-coupling terms in Eq. (1b), we need to add the higher gradient terms in Eq. (1c) and (1d), too. Note that the structure of gradient terms in Eqs. (1b)–(1d) is a principal difference of this paper in comparison with McMillan [1,2], Wandel *et al.* [5], and She

et al. [13]. They did not consider gradient-coupling terms and higher gradients, both of which, as it will be shown below, can have a critical influence on the appearance and stability of separated and coupled spatially modulated phases.

As usual in the Landau approach, the coefficients a_{Si} and a_{Ci} are assumed to depend linearly on the temperature T and change their signs at critical temperatures T_S and T_C:

$$a_{Si}(T) = \alpha_{Si}\left(\frac{T}{T_S} - 1\right), \quad a_{Ci}(T) = \alpha_{Ci}\left(\frac{T}{T_C} - 1\right), \tag{2}$$

where the coefficients $\alpha_{Si} > 0$ and $\alpha_{Ci} > 0$.

For the thermodynamic stability of a system described by the functional in Eqs. (1a)–(1d), the matrix of coefficients b_{Cij} and b_{Sij} are positively defined; the matrices of higher gradient coefficients v_{Cij} and v_{Sij} should be positively defined, too, because the correlation energy of each subsystem C and S must be positive at high values of each order parameter.

The symmetry of vectors and tensors in Eqs. (1a)–(1d) is defined by the point group symmetry of the high-temperature state of a material. Note that, according to McMillan [1,2], they can be coordinate dependent to reflect the microstructure of the studied material. However, such a spatial dependence is contradictory to the space isotropy in the continuous Landau theory.

Following McMillan [1,2], the variation of a CW electron density ρ can be introduced as

$$\rho(\vec{r}, t) = \rho_0(1 + \mathrm{Re}[\psi_{C1} + \psi_{C2} + \psi_{C3}]), \tag{3}$$

where the subscripts 1, 2, and 3 are the orthogonal crystal axes.

Note that Eq. (3) is specific to the CW, and it shows that an observable physical quantity, namely, a positive electron density ρ, is proportional to the real part of a complex function $\boldsymbol{\psi}_C$. The relative variation of the electron density $\delta\rho = \frac{\rho(\vec{r},t)}{\rho_0} - 1$ is equal to $\mathrm{Re}[\psi_{C1} + \psi_{C2} + \psi_{C3}]$. Equation (3) is like the concentration wave representation of atomic densities. At the same time, the free energy functional in Eqs. (1a)–(1d) is much more general since the complex order parameters $\boldsymbol{\psi}_C$ and $\boldsymbol{\psi}_S$ can describe many physical variables, such as the vectorial concentration wave representation of atomic densities; the scalar charge density; the vector of spontaneous electric polarization in multiaxial ferroelectrics or its component in uniaxial ferroelectrics; polar and antipolar order parameters in ferrielectrics and/or antiferroelectrics; the axial vector of spontaneous magnetization and/or antiferromagnetic long-range order parameter(s) in ferromagnets, ferrimagnets, and/or antiferromagnets; and the axial vector(s) of aniferrodistortive long-range order in ferroic and multiferroic materials with spatially modulated phases. We treated the long-range orders as complex variables because this representation allows for a much easier and convenient way to find corresponding wave periods and amplitudes in the spatially modulated SW, CW, and SCW phases.

For the sake of simplicity, below, we consider the one-component 1D case: $\boldsymbol{\psi}_C(\vec{r}) \equiv \psi_C(x)$ and $\boldsymbol{\psi}_S(\vec{r}) \equiv \psi_S(x)$, which allows us to omit all subscripts in Eqs. (1a)–(1d), (2), and (3) and significantly simplify the analysis of the thermodynamic stability conditions. In the one-component 1D, the free energy in Eqs. (1a)–(1d) is stable at high values of the order parameters under the conditions:

$$b_C > 0, \quad b_S > 0, \quad \eta > -2\sqrt{b_S b_C}. \tag{4a}$$

Under these conditions, the free energy in Eqs. (1a)–(1d) can describe several spatially homogeneous phases, namely, the disordered (D) phase, spontaneous long-range (S) and charge density (C) orderings, their coexistence (S/C), and the mixed (SC) state.

For a correct description of the spatially modulated phases, CW, SW, and SCW, the free energy in Eqs. (1a)–(1d) should be stable at high values of the order parameter gradients, which is possible if the parameters simultaneously satisfy the following conditions:

$$\begin{aligned} &v_S > 0, \quad w_S > 0, \quad v_C > 0, \quad w_C > 0, \\ &\chi > -2\sqrt{v_S v_C}, \quad \xi > -2\sqrt{w_S w_C}. \end{aligned} \tag{4b}$$

The conditions

$$g_S > 0, \quad g_C > 0 \tag{4c}$$

make the appearance of the decoupled CW or SW waves less favorable in comparison with homogeneous C or S phases. The set of the stable phases that satisfy the condition in Eqs. (4a)–(4c) are described in Table I.

Analytical description of the order parameter and charge density modulation in the SW-C, CW-S, and SCW phases is possible within a harmonic approximation for the spatial profile of the wave:

$$\begin{aligned} \psi_S &= \delta\psi_{S0} + \delta\psi_S \exp(\pm ikx), \\ \psi_C &= \delta\psi_{C0} + \delta\psi_C \exp(\pm iqx). \end{aligned} \tag{5}$$

Here, the expressions for the bases $\delta\psi_{S0}$ and $\delta\psi_{C0}$, modulation amplitudes $\delta\psi_S$ and $\delta\psi_C$, wave vectors k and q, and energies of the modulated phase follow from the minimization of the free energy in Eqs. (1a)–(1d), which acquires a simple form given by Eq. (A.1b) in Appendix S1 in the Supplemental Material [32]. The minimization conditions $\frac{\delta F}{\delta q} = 0$ and $\frac{\delta F}{\delta k} = 0$ lead to the system of equations for k and q, which in addition to the trivial solution $q = 0$ and/or $k = 0$ can have nontrivial solutions $q \neq 0$ and/or $k \neq 0$.

Note that the wave phases are decoupled in the harmonic approximation in Eq. (5); their coupling can appear when one accounts for anharmonicity. The decoupling leads to the virtual independence of the different modulation periods k and q. Also, we did not find ripples in this paper, corresponding to the simultaneous validity of inequalities $\delta\psi_{S0} \neq 0$ and $\delta\psi_S \neq 0$ (and/or $\delta\psi_{C0} \neq 0$ and $\delta\psi_C \neq 0$) in Eq. (5). We conclude that such states exist for very narrow ranges of parameters which do not allow analytical description and are rarely observable. Due to the absence of ripples, and in accordance with Eq. (3) and Table I, the observable density of CW is proportional to $|\delta\psi_C|\cos(qx)$. The observable quantity corresponding to the S order is determined by its physical nature, e.g., the density of the Cooper pairs is proportional to the wave function density $|\psi_S|^2$, while a spatial modulation of a specific antiferrodistortion can be proportional to $|\delta\psi_S|\cos(kx)$.

TABLE I. Possible thermodynamically stable phases of the free energy in Eq. (7).

Phase/order	Order parameters values or/and amplitudes	Free energy density	Stability conditions
Disordered (D)	$\varphi_C = \varphi_S = 0$	0	$\theta_C > 0, \theta_S > 0$
Homogeneous spontaneous order (S)	$\varphi_S = \pm\sqrt{-\theta_S}, \varphi_C = 0$	$f_{S0} = -\vartheta\frac{\theta_S^2}{4}$	$f_{S0} = \min, \theta_S < 0$
Homogeneous charge ordering (C)	$\varphi_C = \pm\sqrt{-\theta_C}, \varphi_S = 0$	$f_{C0} = -\frac{\theta_C^2}{4}$	$f_{C0} = \min, \theta_C < 0$
Mixed homogeneous S and C orderings (SC)	$\varphi_C = \pm\sqrt{\vartheta\frac{\eta^*\theta_S-\theta_C}{\vartheta-\eta^{*2}}}, \varphi_S = \pm\sqrt{\frac{\eta^*\theta_C-\vartheta\theta_S}{\vartheta-\eta^{*2}}}$	$f_{SC} = -\vartheta\frac{\theta_C^2-2\eta^*\theta_C\theta_S+\vartheta\theta_S^2}{4(\vartheta-\eta^{*2})}$	$f_{SC} = \min, \frac{\eta^*\theta_S-\theta_C}{\vartheta-\eta^{*2}} > 0, \frac{\eta^*\theta_C-\vartheta\theta_S}{\vartheta-\eta^{*2}} > 0$
Spontaneous (superconductive, polar or magnetic) long-range order waves (SW)	$\varphi_C = 0, \varphi_S = \pm\sqrt{2\frac{w_S^*-2v_S^*\theta_S}{4v_S^*-w_S^{*2}}}, k_S = \sqrt{\frac{-2+w_S^*\theta_S}{w_S^*-2v_S^*\theta_S}}.$	$f_{SW} = \vartheta\frac{\theta_S(w_S^*-v_S^*\theta_S)-1}{4v_S^*-w_S^{*2}}$, where $\theta_S = \frac{T}{T_S} - 1$	$f_{SW} = \min, \frac{w_S^*-2v_S^*\theta_S}{4v_S^*-w_S^{*2}} > 0, \frac{-2+w_S^*\theta_S}{w_S^*-2v_S^*\theta_S} > 0$
Charge density waves (CW)	$\varphi_C = \pm\sqrt{2\frac{w_C^*-2v_C^*\theta_C}{4v_C^*-w_C^{*2}}}, q_C = \sqrt{\frac{w_C^*\theta_C-2}{w_C^*-2v_C^*\theta_C}}, \varphi_S = 0$	$f_{CW} = \frac{\theta_C(w_C^*-v_C^*\theta_C)-1}{4v_C^*-w_C^{*2}}$, where $\theta_C = \frac{T}{T_C} - 1$	$f_{CW} = \min, \frac{w_C^*-2v_C^*\theta_C}{4v_C^*-w_C^{*2}} > 0, \frac{w_C^*\theta_C-2}{w_C^*-2v_C^*\theta_C} > 0$
Mixed charge density waves and homogeneous S-order (CW-S)	$\varphi_C = \pm\sqrt{\frac{4\vartheta v_C^*(\theta_C-\eta^*\theta_S)+4\xi_S^*(\eta^*-\theta_C\xi_S^*)+2\vartheta w_C^*(-1+\theta_S\xi_S^*)}{4(\eta^{*2}-\vartheta)v_C^*+\vartheta w_C^{*2}-4\eta^* w_C^*\xi_S^*+4\xi_S^{*2}}}$, $q_C = \sqrt{\frac{-\vartheta w_C^*(\theta_C-\eta^*\theta_S)+2[\vartheta-\eta^{*2}+(\eta^*\theta_C-\vartheta\theta_S)\xi_S^*]}{2\vartheta v_C^*(\theta_C-\eta^*\theta_S)+2\xi_S^*(\eta^*-\theta_C\xi_S^*)+\vartheta w_C^*(\theta_S\xi_S^*-1)}}$, $\varphi_S = \pm\sqrt{\frac{-\vartheta w_C^{*2}\theta_S-4[v_C^*(\eta^*\theta_C-\vartheta\theta_S)+\xi_S^*]+2w_C^*(\eta^*+\theta_C\xi_S^*)}{4(\eta^{*2}-\vartheta)v_C^*+\vartheta w_C^{*2}-4\eta^* w_C^*\xi_S^*+4\xi_S^{*2}}}$, $k_S = 0$	Expression for f_{CW-S} is given by Eq. (S.8)[a]	$f_{CW-S} = \min, q_C > 0, \varphi_C^2 > 0, \varphi_S^2 > 0$
Mixed spontaneous long-range order waves and homogeneous C-order (SW-C)	$\varphi_C = \pm\sqrt{\vartheta\frac{-w_S^{*2}\theta_C+v_S^*(\theta_C-\eta^*\theta_S)-4\xi_C^*+2w_S^*(\eta^*+\theta_S\xi_C^*)}{4(\eta^{*2}-\vartheta)v_S^*+\vartheta w_S^{*2}-4\eta^* w_S^*\xi_C^*+4\xi_C^{*2}}}$, $q_C = 0, \varphi_S = \pm\sqrt{\frac{v_S^*(-4\eta^*\theta_C+4\vartheta\theta_S)-2w_S^*(\vartheta-\theta_C\xi_C^*)+4\xi_C(\eta^*-\theta_S\xi_C^*)}{4(\eta^{*2}-\vartheta)v_S^*+\vartheta w_S^{*2}-4\eta^* w_S^*\xi_C^*+4\xi_C^{*2}}}$, $k_S = \sqrt{\frac{w_S^*(\eta^*\theta_C-\vartheta\theta_S)+2[\vartheta-\eta^{*2}+(\eta^*\theta_S-\theta_C)\xi_C^*]}{2v_S^*(\vartheta\theta_S-\eta^*\theta_C)-w_S^*(\vartheta-\theta_C\xi_C^*)+2\xi_C(\eta^*-\theta_S\xi_C^*)}}$	Expression for f_{SW-C} is given by Eq. (S.9)[a]	$f_{SW-C} = \min, k_S > 0, \varphi_C^2 > 0, \varphi_S^2 > 0$
Intertwined or coupled waves of S and C orders (SCW)	$\varphi_C = \pm\sqrt{\frac{\Delta_C}{\Delta}}, q_C = \sqrt{\frac{\Delta_q}{\Delta_C}}, \varphi_S = \pm\sqrt{\frac{\Delta_S}{\Delta}}, k_S = \sqrt{\frac{\Delta_k}{\Delta_S}}.$	Expressions for f_{SCW}, Δ, Δ_C, Δ_q, Δ_S, and Δ_k are given by Eq. (S.10)[a]	$f_{SCW} = \min, \frac{\Delta_C}{\Delta} > 0, \frac{\Delta_S}{\Delta} > 0, \frac{\Delta_C}{\Delta} > 0, \frac{\Delta_S}{\Delta} > 0$

[a]In the Supplemental Material [32].

III. PHASE DIAGRAM OF THE CONSIDERED SYSTEM

Let us analyze the phase diagram. First, we introduce the dimensionless order parameter amplitudes and wave numbers in the free energy in Eqs. (1a)–(1d):

$$\varphi_C^2 = \frac{|\psi_C|^2}{\psi_{C0}^2}, \quad \varphi_S^2 = \frac{|\psi_S|^2}{\psi_{S0}^2}, \quad q_C = \sqrt{\frac{g_C}{\alpha_C}}q, \quad k_S = \sqrt{\frac{g_S}{\alpha_S}}k, \tag{6a}$$

where $\psi_{C0}^2 = \frac{\alpha_C}{2b_C}$ and $\psi_{S0}^2 = \frac{\alpha_S}{2b_S}$. Also, we introduce the following dimensionless parameters, gradient coefficients, and biquadratic coupling constants:

$$f_C = \frac{\alpha_C^2}{b_C}, \quad f_S = \frac{\alpha_S^2}{b_S}, \quad \vartheta = \frac{f_S}{f_C}, \tag{6b}$$

$$v_C^* = \frac{v_C}{b_C}\left(\frac{\alpha_C}{g_C}\right)^2, \quad v_S^* = \frac{v_S}{b_S}\left(\frac{\alpha_S}{g_S}\right)^2,$$

$$w_C^* = \frac{w_C}{b_C}\frac{\alpha_C}{g_C}, \quad w_S^* = \frac{w_S}{b_S}\frac{\alpha_S}{g_S}, \tag{6c}$$

$$\eta^* = \frac{\alpha_C\alpha_S}{2b_Cb_S}\frac{\eta}{f_C}, \quad \xi_S^* = \frac{\alpha_C\alpha_S}{2b_Cb_S}\frac{\xi}{f_C}\frac{\alpha_S}{g_S},$$

$$\xi_C^* = \frac{\alpha_C\alpha_S}{2b_Cb_S}\frac{\xi}{f_C}\frac{\alpha_C}{g_C}, \quad \chi^* = \chi\frac{(\alpha_C\alpha_S)^2}{2b_Cb_S}\frac{\xi}{f_C}\frac{1}{g_Cg_S}. \tag{6d}$$

Using the dimensionless variables and order parameters in Eqs. (6a)–(6d), we rewrite Eqs. (1a)–(1d) as

$$\frac{f}{f_C} = \left[\theta_C(T, q_C)\frac{\varphi_C^2}{2} + \beta_C(q_C)\frac{\varphi_C^4}{4}\right] + \vartheta\left[\theta_S(T, k_S)\frac{\varphi_S^2}{2} + \beta_S(k_S)\frac{\varphi_S^4}{4}\right] + \mu(k_S, q_C)\frac{\varphi_C^2\varphi_S^2}{2}, \tag{7}$$

where we introduced the temperature- and wave-number-dependent dimensionless functions:

$$\theta_C(T, q_C) = \frac{T}{T_C} - 1 + q_C^2,$$

$$\theta_S(T, k_S) = \frac{T}{T_S} - 1 + k_S^2, \tag{8a}$$

$$\beta_C(q_C) = 1 + w_C^* q_C^2 + v_C^* q_C^4,$$
$$\beta_S(k_S) = 1 + w_S^* k_S^2 + v_S^* k_S^4, \quad (8b)$$
$$\mu(k_S, q_C) = \eta^* + \xi_S^* k_S^2 + \xi_C^* q_C^2 + \chi^* k_S^2 q_C^2. \quad (8c)$$

The free energy in Eq. (7) depends on the S to C subsystem energy ratio ϑ, whose magnitude can be arbitrary: small, close to unity, or large; and these cases are analyzed below. The functions $\theta_C(T, q_C)$ and $\theta_S(T, k_S)$ are the reduced temperatures of C and S subsystems renormalized by the gradient energy of each order parameter. Positive functions $\beta_C(q_C)$ and $\beta_S(k_S)$ are fourth-order nonlinearity of C and S subsystems renormalized by the gradient energy of each order parameter. The function $\mu(k_S, q_C)$ is the biquadratic coupling of S and C subsystems renormalized by the gradient coupling parameters ξ_S^*, ξ_C^*, and χ^*, and wave numbers k_S^2 and q_C^2.

The free energy in Eq. (7) is stable at high values of order parameters and wave numbers if the following conditions are simultaneously satisfied:

$$\eta^* > -\sqrt{\vartheta}, \quad \xi_C^* > -\sqrt{v_C^*}, \quad \xi_S^* > -\sqrt{\vartheta v_S^*},$$
$$\chi^* > -\sqrt{\vartheta v_C^* v_S^*}, \quad w_C^* > -\sqrt{4 v_S^*}, \quad w_C^* > -\sqrt{4 v_C^*}. \quad (9)$$

Since the conditions in Eqs. (4a)–(4c) are satisfied, the last three inequalities are valid, too.

The free energy in Eq. (7) allows us to derive analytical expressions for the energies of different phases, the amplitudes of the corresponding order parameters and charge density waves, and modulation periods. Thermodynamically stable homogeneous phases and spatially modulated states of the energy in Eq. (7), corresponding absolute values of the order parameters, phase energies, and stability conditions are listed in Table I.

Using analytical expressions from Table I, one can calculate the phase diagrams of various ferroics and high-T_c superconductors with charge order, lattice/electronic long-range order parameters, CW amplitudes, and modulation periods. Note that the relative density $\delta\rho$ of CW is proportional to $|\varphi_C|\cos(qx)$ in accordance with Eq. (3).

A concrete view of phase diagrams and related properties are determined by 11 dimensionless parameters: a constant of the S-C biquadratic coupling strength η^*; three constants of the biquadratic gradient-coupling strength ξ_S^*, ξ_C^*, and χ^*; four gradient coefficients of S and C subsystems v_C^*, v_S^*, w_C^*, and w_S^*; their energy ratio ϑ; and two temperature ratios $\frac{T}{T_C}$ and $\frac{T}{T_S}$, respectively. Since we are mostly interested in the conditions of the spatially modulated phase stability at corresponding equilibrium wave numbers, we can take all possible measures to reduce the number of dimensionless parameters in the energy in Eq. (7). For further reduction of the number of independent parameters up to eight, we analyzed the realistic case:

$$\xi_S^* = \xi_C^* = \xi^*, \quad v_C^* = v_S^* = v^*, \quad \text{and} \quad w_C^* = w_S^* = w^*. \quad (10)$$

Putting $T \to 0$, we can exclude two transition temperatures T_S and T_C from our consideration. As a result, the obtained six-parametric LG model is not much more complex than earlier LG models for two coupled long-range orders with respect to the number of fitting parameters.

The remaining six parameters η^*, ξ^*, ϑ, χ^*, v^*, and w^* can provide a comprehensive deconvolution of versatile experimental data and are suitable for their Bayesian analysis and machine learning. The phase diagram, order parameter amplitudes, and modulation periods are most sensitive to the parameters η^* and ξ^* (which can change their sign) and ϑ, and less sensitive to the positive parameters χ^*, v^*, and w^*. Several cases are presented and analyzed below.

Typical dependence of the free energy in Eq. (7) on the order parameter amplitudes φ_C and φ_S, shown in Figs. 1(a)–1(d), is the appearance of the stable mixed SC phase at $\mu \leqslant 0$ independently on ϑ values. The coexistence of the S and C phases with relatively deep energy minima is possible only for $\vartheta = 1$ and $\mu > 1$; the stable S or C phase with deep energy minima appears at $\mu > 0$, and $\vartheta \gg 1$ or $\vartheta \ll 1$, respectively (see also Figs. S1–S3 in the Supplemental Material [32]).

A typical phase diagram as a function of η^* and ϑ, calculated from the free energy in Eq. (7) for $T = 0$, $\chi^* = 1$, $v^* = 10$, $w^* = 0.1$, and $\xi^* = -1$, is shown in Fig. 1(e). Stable ordered phases are absent in the white region, where the inequality $\eta^* > -\sqrt{\vartheta}$ is invalid, and a system described by the free energy in Eq. (7) is unstable. A relatively narrow stripe-shaped dark green region of the SCW phase is located inside the largest light green region of the SC state. Note that the area of the spatially modulated CW-S, SW-C, and SCW phases for $\eta^* \leqslant 0$ decreases monotonically with decrease in $|\xi^*|$, and the phases almost disappear at $\xi^* \approx -0.20$ (see Fig. S4 in Appendix S3 in the Supplemental Material [32]). The area of the homogeneous SC phase increases monotonically with ξ^* increase from -1 to -0.25; and the phase occupies the regions of the modulated phases at more negative ξ^*. The location and area of the homogeneous S and C phase regions are independent of ξ^*. The S phase is stable at $\vartheta > 1$; the C phase is stable at $\vartheta < 1$, and the boundary between them is a horizonal line $\vartheta = 1$, as anticipated from Table I.

Dimensionless wave numbers q_C and k_S, corresponding to the diagram in Fig. 1(e), are shown in Figs. 1(g)–1(h), as a function of η^* and ϑ. The wave numbers can be nonzero in the spatially modulated phases and are different $q_C \neq k_S$ wherever $\vartheta \neq 1$. The wave number q_C is nonzero in the SCW and CW-S phases, and k_S is nonzero in the SCW and SW-C phases. The wave number q_C tends to zero at the boundary between the CW-S and SC phases and between the SCW and SW-C phases; it continuously changes across the CW-S and SCW border, increases strongly, and reaches maxima at the boundary of the SCW phase with the unstable white region. The wave number k_S tends to zero at the border between the SCW and CW-S phases; it continuously changes across the boundary between the SW-C and SCW phases and increases strongly approaching the boundary between the SW-C and SC phases.

Normalized order parameters (or their amplitudes in the spatially modulated phases) φ_C and φ_S are shown in Figs. 1(k) and 1(l) as a function of η^* and ϑ. As anticipated, the parameter φ_C is zero in the S phase, and φ_S is zero in the C phase. Both parameters are nonzero in the SCW, CW-S, SW-C, and SC phases, where their amplitudes are relatively small in comparison with the values near the boundary with the unstable region, where the order parameters formally diverge (see also Fig. S5 in the Supplemental Material [32]).

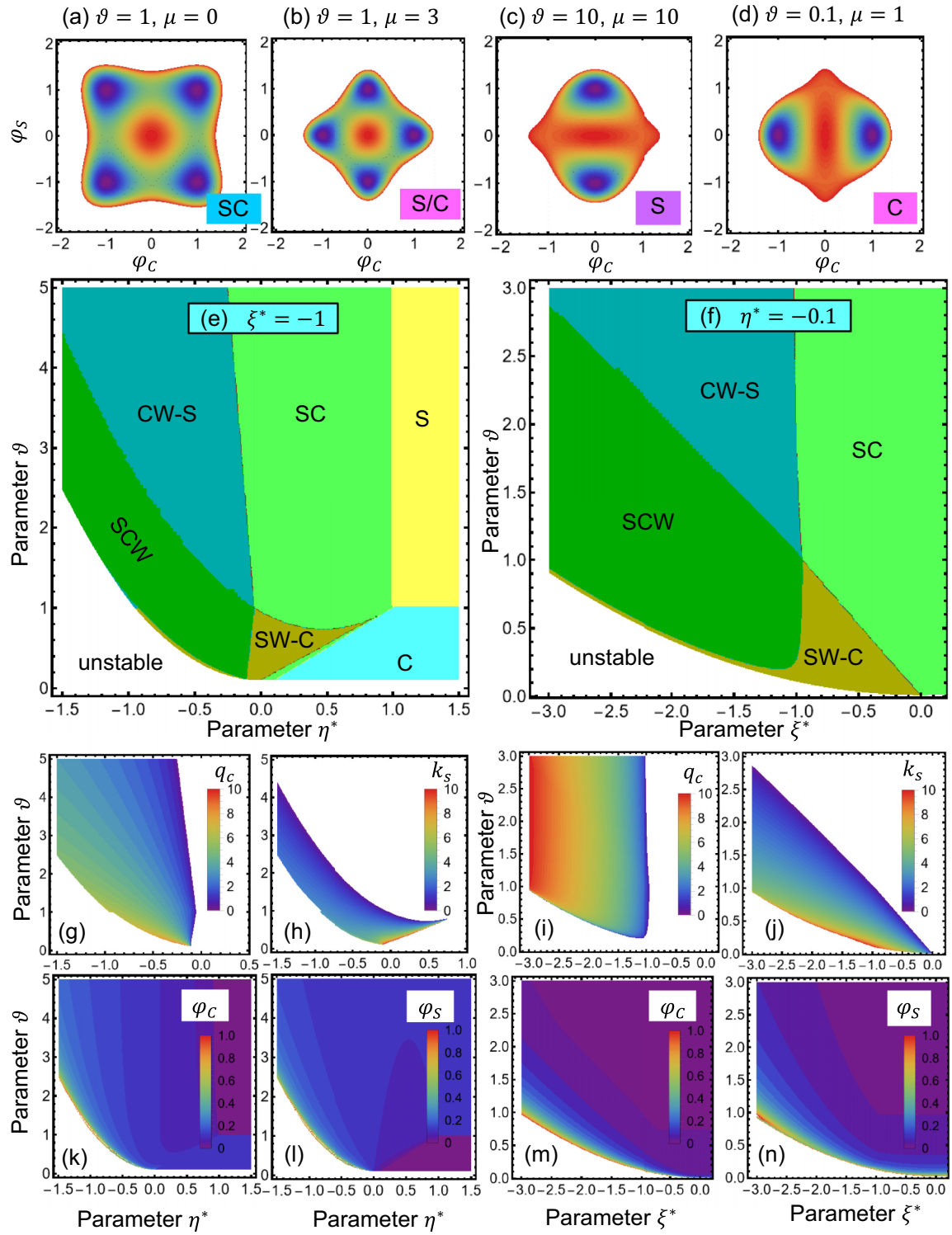

FIG. 1. (a)–(d) The free energy in Eq. (7), as a function of order parameter amplitudes φ_C and φ_S, calculated for different values of dimensionless parameters ϑ and μ listed near the plots. Red color denotes zero energy, while violet color is its minimal density in relative units. (e) and (f) Phase diagrams, corresponding dimensionless wave numbers (g) and (i) q_C and (h) and (j) k_S, and normalized order parameters (or/and their amplitudes in the modulated phases) (k) and (m) φ_C and (l) and (n) φ_S, as a function of coupling constants ξ^* or η^* and ϑ, calculated for $T = 0$, $\chi^* = 1$, $v^* = 10$, $w^* = 0.1$, and $\xi^* = -1$ for plots (e), (g), and (h) and $\eta^* = -0.1$ for plots (f), (i), and (j). Capital letters in the plots (a)–(d), (e), and (f) denote the mixed spontaneous long-range order charge order state (SC), their coexistence (S/C), spontaneous long-range order (S) and its waves (SW), charge ordered (C) states and charge density waves (CW), and intertwined long-range order charge density waves (SCW), respectively.

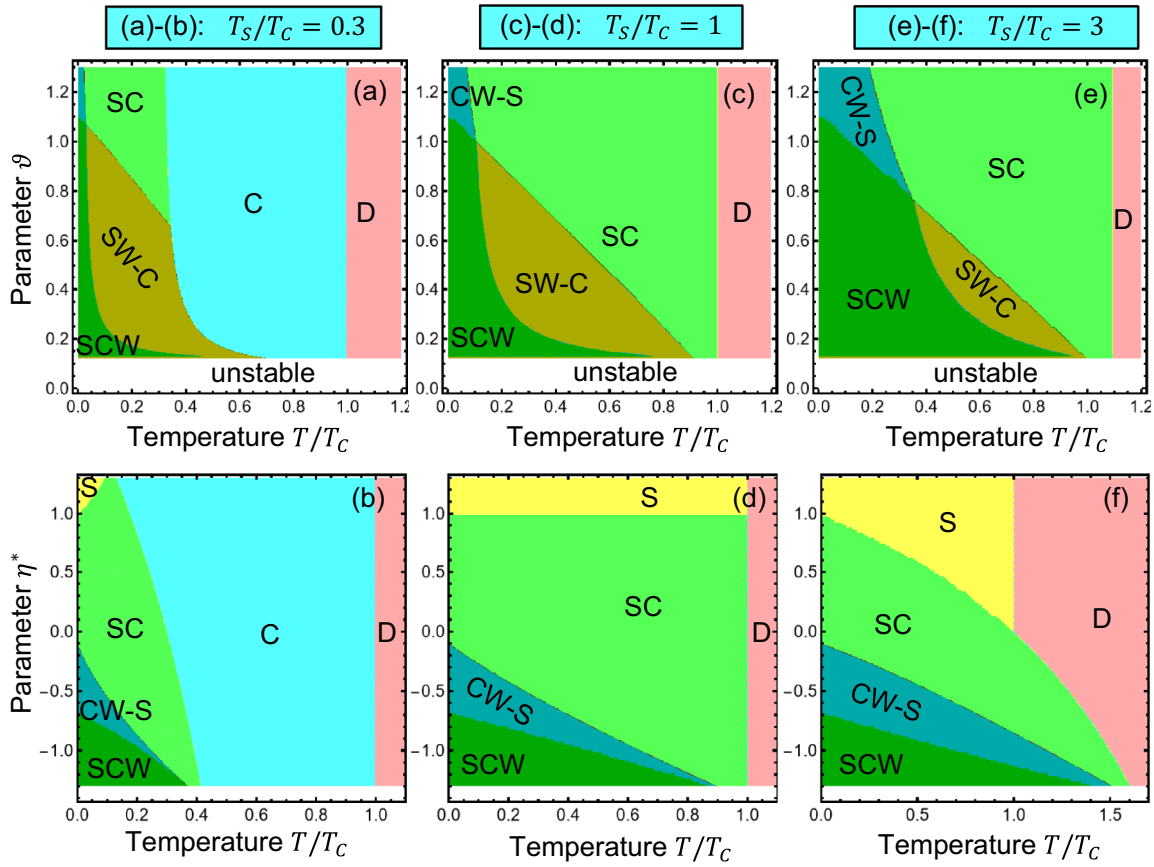

FIG. 2. (a), (c), and (e) Phase diagrams in coordinates $T-\vartheta$ calculated for $\eta^* = -0.15$. (b), (d), and (f) Phase diagrams in coordinates $T-\eta^*$ calculated for $\vartheta = 2$. Other parameters: (a) and (b) $T_S/T_C = 0.3$, (c) and (d) $T_S/T_C = 1$, (e) and (f) $T_S/T_C = 3$; $\xi^* = -1$, $\chi^* = 1$, $v^* = 10$, and $w^* = 0.1$.

A typical phase diagram, as a function of ξ^* and ϑ, calculated from the free energy in Eq. (7) for $T = 0$, $\chi^* = 1$, $v^* = 10$, $w^* = 0.1$, and $\eta^* = -0.1$, is shown in Fig. 1(f). Stable phases are absent in the white region, where the inequality $\xi^* > -\sqrt{\vartheta v^*}$ is invalid, and so a system described by the free energy in Eq. (7) is unstable. The dark green region of the SCW phase is largest for higher negative η^*; it decreases monotonically with increase in η^* from negative values to zero; and at the same time, the relatively small region of SW-C phase appears with η^* increase from negative values to zero (see Fig. S6 in the Supplemental Material [32]). The regions of the SC, CW-S, and SW-C phases disappear at $\eta^* \geqslant 1$, being adsorbed by the regions of the S and C phases. A very small triangular region of the SCW phase, located at the S-C boundary $\vartheta = 1$, remains at $\eta^* = 1$ (see Fig. S6(g) in the Supplemental Material [32]).

Dimensionless wave numbers q_C and k_S, corresponding to the diagram in Fig. 1(f), are shown in Figs. 1(i) and 1(j) as a function of ξ^* and ϑ. The wave number q_C is nonzero in the SCW and CW-S phases, and k_S is nonzero in the SCW and SW-C phases. The wave number q_C tends to zero at the boundaries between the CW-S and SC phases and/or between the SCW and SW-C phases; it continuously changes across the CW-S and SCW boundary and increases approaching the boundary of the SCW phase with the unstable white region. The wave number k_S tends to zero at the boundary between the SCW and CW-S phases and/or at the boundary between the SW-C and SC phases; it continuously changes at the SCW and SW-C boundary and increases strongly approaching the boundary between the SW-C phase and the white unstable region (see also Figs. S4(c), S4(f), S4(i) and S6(c), S6(f), S6(i) in the Supplemental Material [32]).

Normalized order parameters (or/and their amplitudes in the spatially modulated phases) φ_C and φ_S are shown in Figs. 1(m) and 1(n) as a function of ξ^* and ϑ (see also the middle and bottom rows of Fig. S7 in the Supplemental Material [32]). As anticipated, the parameter φ_C is zero in the S phase, and φ_S is zero in the C phase. Both parameters are nonzero in the SCW, CW-S, SW-C, and SC phases, where their amplitudes are relatively small in comparison with the values near the boundary of the SCW and/or SW-C phases with the unstable white region, where the order parameters formally diverge. Since the order parameters strongly increase when approaching the boundary with the unstable region, here, the accuracy of harmonic approximation, used by us for the description of the long-range order in the spatially modulated phases SCW, SW-C, and CW-S, becomes very low, and this questions its applicability. Therefore, a very narrow region of the SW-C phase, which exists between the SCW phase and the white unstable region in Figs. 1(e) and 1(f), not being a numerical error, is rather an artifact related with the overestimation of model applicability limits.

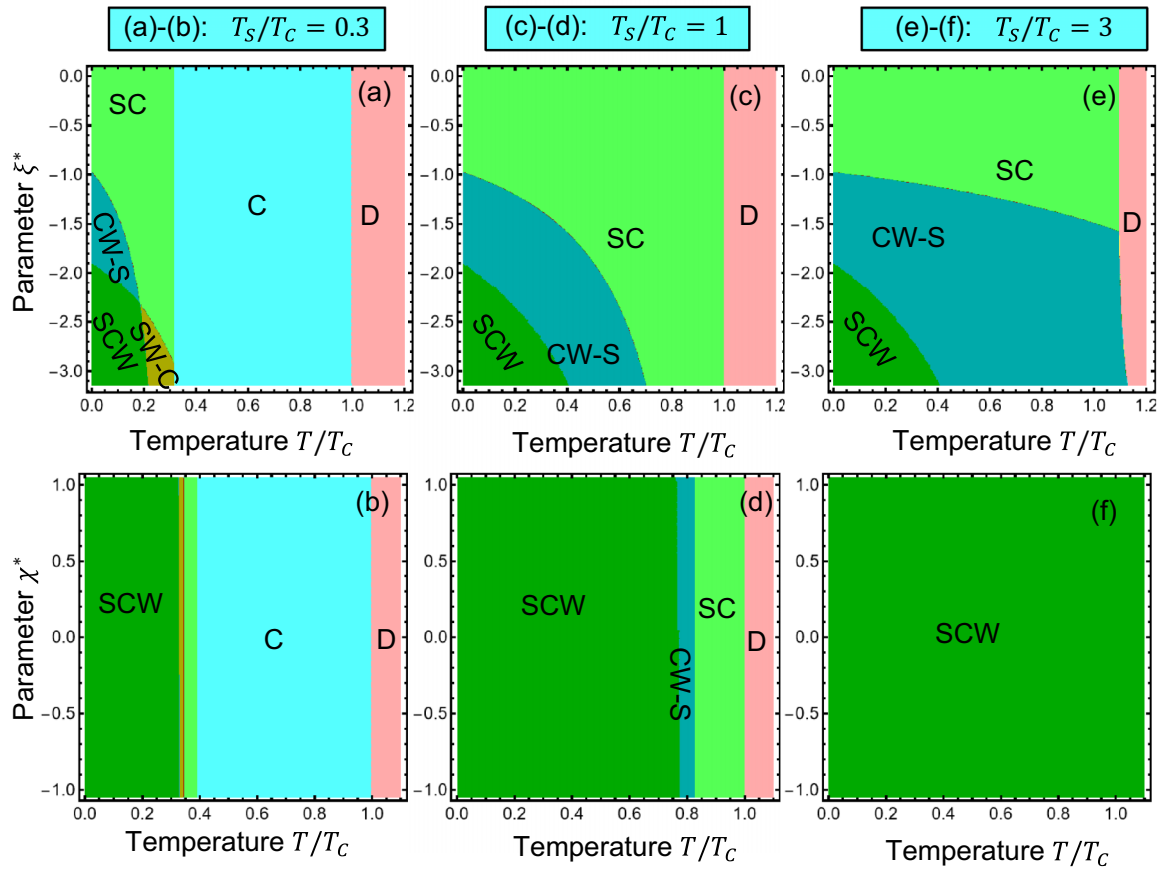

FIG. 3. (a), (c), and (e) Phase diagrams in coordinates $T - \xi^*$ calculated for $\chi^* = 1$, $\eta^* = -0.15$, and $\vartheta = 2$. (b), (d), and (f) Phase diagrams in coordinates $T - \chi^*$ calculated for $\vartheta = 2$ and $\eta^* = -1, \xi^* = -2$. Other parameters: (a) and (b) $T_S/T_C = 0.3$, (c) and (d) $T_S/T_C = 1$, (e) and (f) $T_S/T_C = 3$; $v^* = 10$, and $w^* = 0.1$.

Results presented above correspond to very low temperatures $0 \leqslant T \ll \min[T_C,\ T_S]$. The values of T_C and/or T_S can play a very significant role when the temperature T rises and becomes comparable with $\min[T_C,\ T_S]$. We hope to consider this question in detail in the near future. Preliminary calculations for higher temperatures, some results of which are presented in Figs. 2 and 3, show that the ratio $T_C/\ T_S$ has a principal influence on the form of the phase diagrams. The temperature dependence of phases is very sensitive to the parameters η^* and ϑ, relatively sensitive to the parameter ξ^*, and almost insensitive to the positive parameter χ^* for given values of v^* and w^*.

IV. NONLINEAR CHARGE DENSITY WAVES AND COMPLEX TOPOLOGICAL STRUCTURES

Note that the phase boundaries of the spatially modulated phases, shown in Fig. 1 and Figs. S4–S7 in Appendix S3 in the Supplemental Material [32], are calculated within the harmonic approximation in Eq. (5), which is valid near the boundaries of the second-order phase transitions, where the CW profiles are sinusoidal or soft. When one moves deeper into the spatially modulated phase region, the harmonic approximation becomes invalid, and the wave profiles become anharmonic. In the simplest 1D case, a sinusoidal wave profile becomes harder and transforms into nonlinear elliptic functions, e.g., in an elliptic sine (snoid). In more complex 2D and three-dimensional (3D) cases, versatile topological structures (e.g., vortices, merons, skyrmions, and labyrinths) and other topological defects (e.g., ribbons, random spots, and bubbles) can appear spontaneously near impurity atoms and/or vacancies, surfaces, and/or interfaces. They are long-living metastable configurations, which minimize the system electrostatic energy. Within the framework of the proposed LG model, the appearance of the topological features is controlled by the structure and magnitude of the gradient terms in Eqs. (1b)–(1d), often being a gradient-induced morphological phase transition [33].

Let us underline that the structure of gradient terms in Eqs. (1b)–(1d) is more complete in comparison with earlier Landau-type models [1,2,13] because corresponding gradient terms in the expressions in Eqs. (1b) and (1c) include the same as well as additional terms. Due to the additions, which have critical influence on the appearance and stability of separated and coupled spatially modulated phases, the proposed LG model describes more scenarios of the CW coexistence, competition, or spatial separation with the other long-range order S in comparison with the models [1,2,13], and so it can potentially describe more experimental data.

Wandel *et al.* [5] consider a different gradient term $\frac{1}{2mQ^2}|\mathbf{Q}\cdot(\nabla\alpha - i\mathbf{Q})|^2$, which includes the gradient of the real dimensionless order parameter α and the wave vector

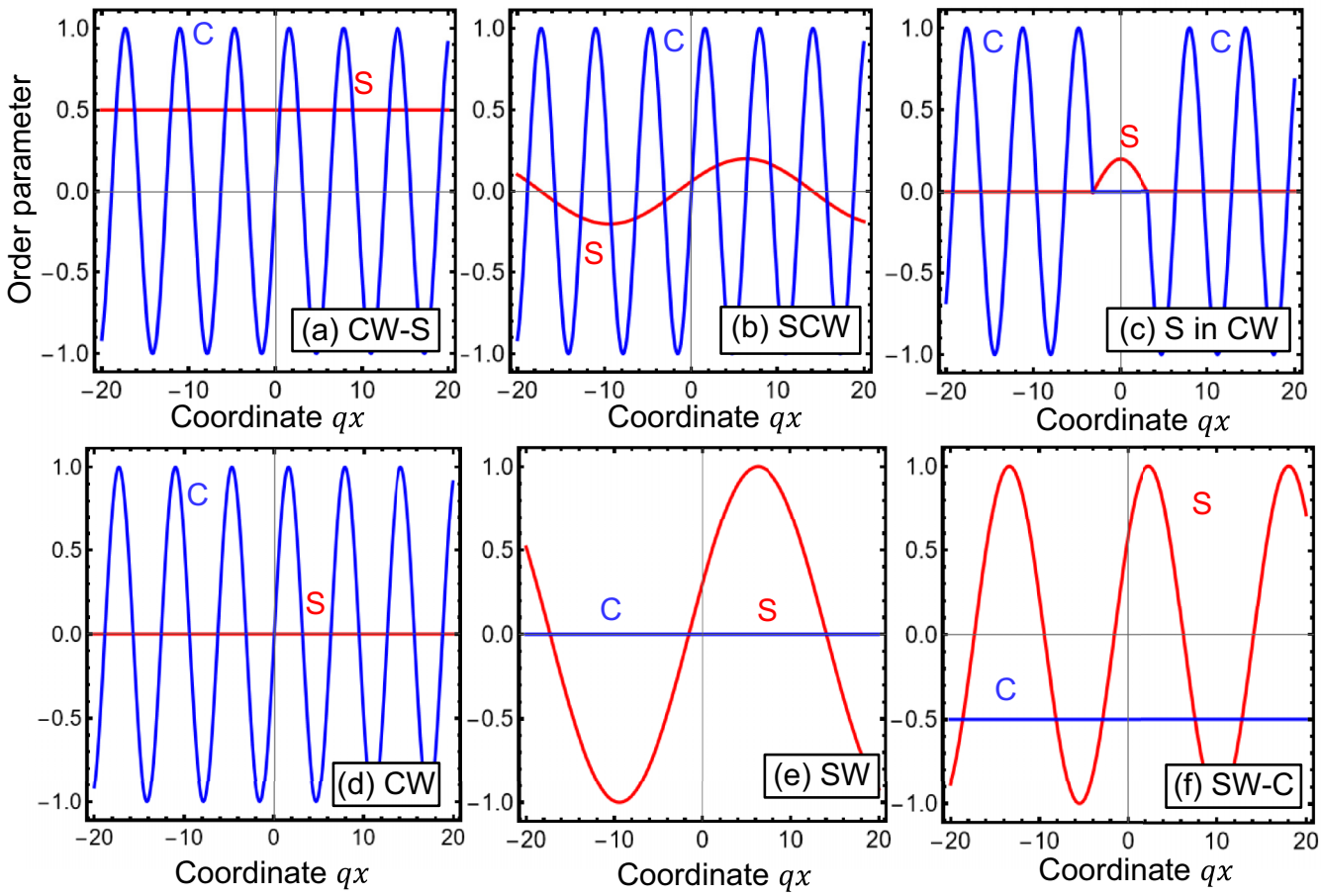

FIG. 4. Schematical illustrations of (a) coexisting homogeneous S and CW orders in the CW-S phase; (b) the spatially modulated S and C waves in the SCW phase; (c) the S phase region inside the CW phase. The spatially modulated (d) CW, (e) SW, and (f) SW-C phases. Red and blue curves are $\mathrm{Re}[\psi_S]$ and $\mathrm{Re}[\psi_C]$, respectively.

Q related to the wavelength of incommensurate CW. The expression may be a particular case of more general expressions $g_{Cij}|\frac{\partial\psi_{Ci}}{\partial x_j}|^2$ and $g_{Sij}|\frac{\partial\psi_{Si}}{\partial x_j}|^2$ included in Eqs. (1c) and (1d) [34]. Wandel *et al.* [5] observe the enhancement of the CW spatial coherence in the high-T_c superconducting cuprate $YBa_2Cu_3O_{6+x}$ triggered by the laser-driven quench of the superconducting state and discussed three possible scenarios of the superconductivity-CW interaction. As the first scenario, they consider the time-dependent LG (TDLG) model to interpret the dynamical interplay between interacting orders, assuming locally coexisting orders. In their formulation, which predicts homogenous and competitive superconductive and charge orders, the CW order parameter amplitude would increase on a picosecond timescale, driven by the quench of superconductivity. The result was in principal disagreement with their observations, where the signal was dominated by a change of correlation length. They conclude that a simple competition model is incompatible with experimental results. Their second scenario considers phase-separated strongly competitive orders using modified McMillan [1,2] formalism. In this case, well-separated CW and superconducting domains, with an average spacing between neighboring CW domains larger than the CW periodicity, also remains incompatible with the experimental data. The third hypothesis, which explained their observations well, is a superconductive region acting as a topological defect (e.g., dislocation) inside the CW region before photoexcitation. The topological defect induces a phase shift of the CW pattern, which propagates from the core of the defect, until the sudden photo-quench of superconductivity removes the defect.

Within harmonic approximation, the proposed LG model describes coexisting CW and S order, abbreviated as the CW-S phase and shown schematically in Fig. 4(a). The spatially modulated S and C waves, in which phase and periods are decoupled in the harmonic approximation, are shown schematically in Fig. 4(b). The spatially separated S and C domains, which may look like small S-phase regions inside the CW phase (or vice versa), can appear at the morphotropic boundary between the C and S phases [shown schematically in Fig. 4(c)]. All these scenarios are possible at $\eta^* < 0$, $\xi^* < 0$, and $\vartheta > 1$.

Anharmonicity and strong nonlinearity can change the situation, shown in Figs. 4(b) and 4(c), and the low-dimensional spatially separated S domains can behave as 1D, 2D, or 3D topological defects for CWs. To study the equilibrium states of spatially inhomogeneous structures, such as the topological defects, in materials with coupled long-range orders, numerical modeling based on the minimization of the free energy in Eqs. (1a)–(1d) is required. Allowing for the Khalatnikov mechanism of the order parameter relaxation, minimization

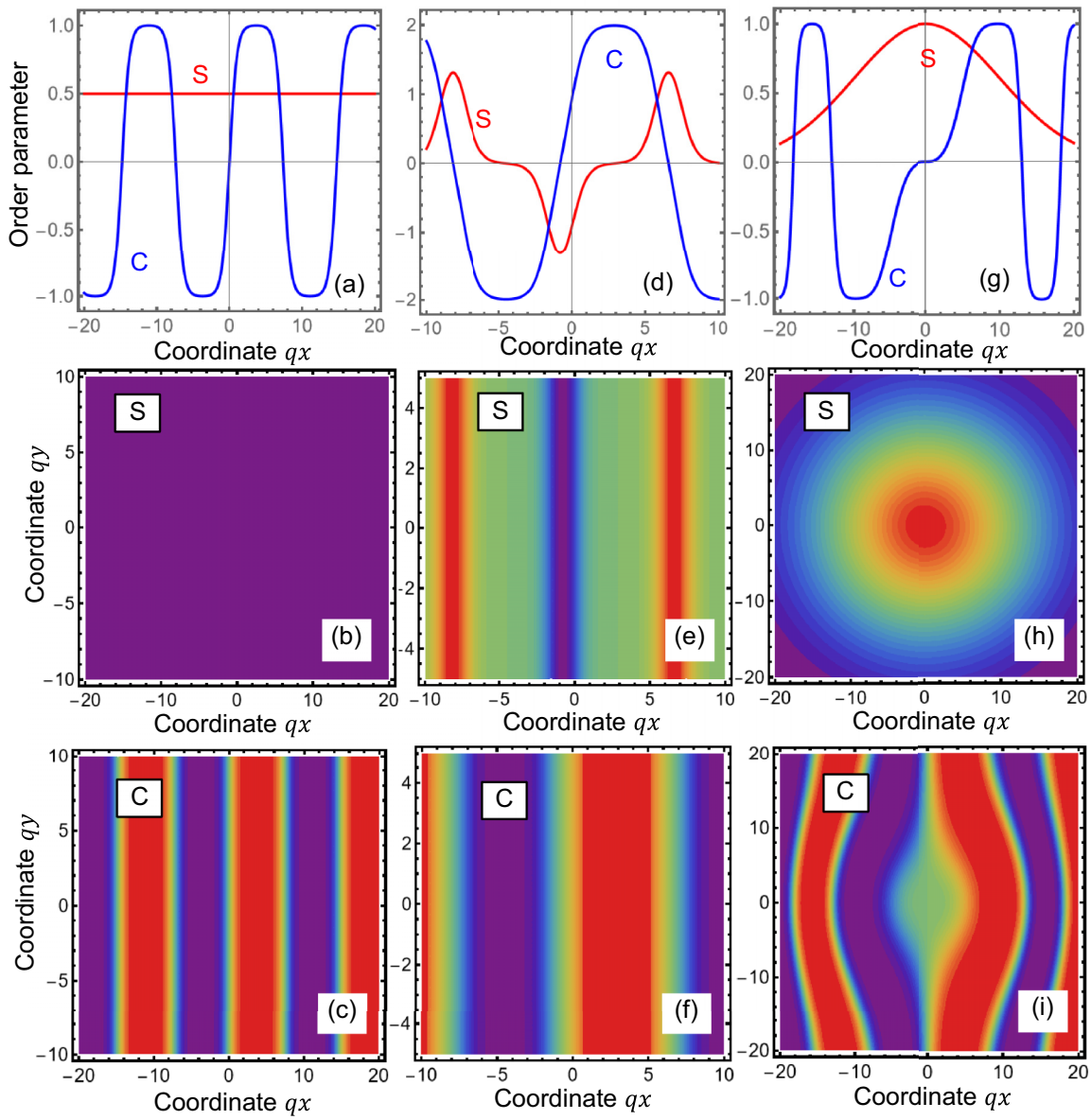

FIG. 5. (a)–(c) Schematical illustrations of the coexisting homogeneous S and CW orders, (b)–(f) the anharmonic coupled waves of S and C orders, and (g)–(i) the localized spot of S regions, which disturbs the phase of CW. Red curves in plots (a)–(c) are φ_S, and blue curves are φ_C.

of the free energy in Eqs. (1a)–(1d) with respect to the order parameters $\boldsymbol{\psi}_C^*$ and $\boldsymbol{\psi}_S^*$ leads to the coupled TDLG relaxation equations:

$$-\Gamma\frac{\partial\boldsymbol{\psi}_C}{\partial t}=\frac{\delta F[\boldsymbol{\psi}_C,\ \boldsymbol{\psi}_S]}{\delta\boldsymbol{\psi}_C^*},\quad -\Gamma\frac{\partial\boldsymbol{\psi}_S}{\partial t}=\frac{\delta F[\boldsymbol{\psi}_C,\ \boldsymbol{\psi}_S]}{\delta\boldsymbol{\psi}_S^*}. \quad (11)$$

Here, the dissipation constant Γ is the Landau-Khalatnikov relaxation coefficient [35]. The TDGL Eq. (11) is used in the finite element modeling (FEM) of the S and C order parameter relaxation from a given initial distribution (e.g., from some regular structure or, more often, randomly small fluctuations) to equilibrium spatially inhomogeneous structures. FEM, as well as more powerful phase-field modeling [36], based on TDLG equations is a usual tool for numerical search of equilibrium spatially inhomogeneous structures. The approach is widely used for the description of 2D and 3D domain structures of various morphology (stripes, vortices, labyrinths, bubbles, halos, topological defects, etc.) in different materials with coupled long-range orders [36].

Since we are interested in the form of equilibrium structure only, the value of Γ does not play any role when the simulation time t is much higher than the maximal of characteristic relaxation times $\tau_S=\frac{\Gamma}{|a_S|}$ and $\tau_C=\frac{\Gamma}{|a_C|}$ because initial distributions of the C and S order parameters eventually relax to the equilibrium state. The condition $t\gg\max[\tau_S,\tau_C]$ can be fulfilled everywhere except for the immediate vicinity of transition temperatures T_S or T_C, where a_S or a_C tends to zero. Thus, at low temperatures considered in this paper, the dimensionless machine time can be introduced as $\tau=\frac{t}{\tau_{LK}}$, where $\tau_{LK}=\max[\frac{\Gamma}{|\alpha_S T_S|},\frac{\Gamma}{|\alpha_C T_C|}]$. The explicit form of the coupled Eq. (11), written in the dimensionless variables, is listed in Appendix S1 in the Supplemental Material [32].

Using these equations, we analyzed different scenarios of decoupled, coupled, and/or intertwined S and C orders; and a schematical illustration some of them is shown in Figs. 5(a), 5(d), and 5(g). Results presented in Fig. 5 correspond to $\tau \gg 10^2$, $\xi_S^* = \xi_C^* = \xi^*$, $v_C^* = v_S^* = v^*$, $w_C^* = w_S^* = w^*$, and $T \to 0$. The top row are profiles calculated at $y = 0$, and the middle and bottom rows are 2D contour maps in $\{x, y\}$ coordinates.

The coexisting homogeneous S order and nonlinear anharmonic CW is shown in Figs. 5(a)–5(c). It appeared that the profile of CW is described well by an elliptic sine function, whose phase is apparently decoupled from the magnitude of the S order. The anharmonic coupled waves of S and C orders are shown in Figs. 5(b)–5(f). It appeared that their profiles, which appeared antiphase, are described well by a combination of elliptic functions. The localized S spot, which disturbs the phase of nonlinear CW, is shown in Figs. 5(g)–5(i). These examples show that S waves and spots can act as 1D and 2D topological defects for the CW.

V. CONCLUSIONS

We propose a LG description of the charge density waves coupled with lattice and/or electronic long-range ordering in ferroics and/or high-temperature superconductors. We derive analytical expressions for the energies of different phases, corresponding order parameters, wave amplitudes, and modulation periods. Using the analytical expressions listed in Table I, one can calculate the phase diagrams of versatile ferroics and high-T superconductors with the charge order C and the spontaneous long-range (superconductive, polar, or magnetic) order parameter S, corresponding amplitudes, and modulation period of charge density waves. The order parameter amplitudes and modulation periods are most sensitive to the biquadratic and biquadratic gradient-coupling strength, which can change their sign, and to the S/C energy ratio and less sensitive to the positive gradient coefficients. The analytical expressions obtained in this paper can be employed to guide the comprehensive physical explanation, deconvolution, and Bayesian analysis of experimental data on quantum materials ranging from charge-ordered ferroics to high-temperature superconductors.

Numerical results presented in this paper are obtained and visualized using a specialized software Mathematica 13.1 [37], and the Mathematica notebook which contains the codes is available per reasonable request.

ACKNOWLEDGMENTS

We are sincerely grateful to the referees for stimulating discussions and very useful suggestions. This paper is supported by the U.S. Department of Energy, Office of Science, Basic Energy Sciences, under Award No. DE-SC0020145 as part of the Computational Materials Sciences Program. A.N.M. and E.A.E. are also supported by the National Academy of Sciences of Ukraine.

The research idea belongs to A.N.M. and L.-Q.C. A.N.M. formulated the problem, performed analytical calculations, analyzed results, and wrote the manuscript draft. E.A.E. wrote codes and prepared figures. V.G. and L.-Q.C. worked on the manuscript improvement.

APPENDIX A: TEMPERATURE-DEPENDENT PHASE DIAGRAMS

Results presented here correspond to very low temperatures $0 \leqslant T \ll \min[T_C,\ T_S]$. The values of T_C and/or T_S can play a very significant role when the temperature T rises and becomes comparable with $\min[T_C,\ T_S]$. We hope to consider this question in detail in the near future. Preliminary calculations for higher temperatures, some results of which are presented in Figs. 2 and 3, show that the ratio $T_C/\ T_S$ has a principal influence on the form of the phase diagrams. The phase diagrams are very sensitive to the parameters η^* and ϑ (see Fig. 2), relatively sensitive to the parameter ξ^* (see Fig. 3, the top row), and almost insensitive to the positive parameter χ^* (see Fig. 3, the bottom row) for given values of v^* and w^*.

APPENDIX B: ESTIMATES OF BIQUADRATIC COUPLING COEFFICIENTS

Our model is still far from the quantitative description of available experiments for SCW in high-temperature superconductors because too many LG parameters are unknown and should be determined from microscopic, e.g., *ab initio*, calculations. Our model may be suitable for the semiquantitative description of CW in ferroics, such as the electronic ferroelectric $LuFe_2O_4$ [38], transition-metal dichalcogenide $TiSe_2$ [39,40] with charge density waves and antiferroelectric instability, and rare-earth tritelluride $LaTe_3$ with light-induced crossed charge density waves along the a and c axes [41], as well as for the description of strongly coupled elastic strain, ferroelectric, and/or superconducting orderings in R-doped incipient ferroelectric $SrTiO_3$ [42,43] (R = Sm, La, Nb, …). For ferroelectric and piezoelectric materials such as $LuFe_2O_4$, low-dimensional $TiSe_2$, and strained $SrTiO_3$, the spontaneous polar and/or antipolar order parameters are either measured and/or calculated by density functional theory [44] or can be estimated from, e.g., piezoelectric reaction. For rare-earth tritellurides such as $LaTe_3$, the transition temperatures T_{C1} and T_{C2} and wave numbers q_{C1} and q_{C2} have been measured. Also, the electronic properties of these materials are relatively well known. The gradient coefficients g_C and g_S can be estimated from the width of domain walls and/or CW modulation periods. Higher-order gradient coefficients w_C and w_S, v_C and v_S can be estimated from the modulation period, and it is reasonable for them to be pairwise equal. The biquadratic coupling parameters η, ξ and χ are poorly known and should be determined (or at least estimated) from available experiments and/or microscopic calculations. Their direct measurements are hardly possible for materials with CW, and we dare to list our indirect estimates in Table II, where the ranges of scattering of parameters are very high and overlap the ranges of dimensionless parameters well, shown in Figs. 2 and 3.

Here, we regard that the long-range parameter ψ_S is a spontaneous (or incipient) polarization P_S, measured in C/m^2. The charge density ρ is normalized as $\rho = \rho_0 \mathrm{Re}[\psi_C]$ [1], where ρ_0 is a homogeneous carrier density (in C/m^2) and ψ_C is a dimensionless charge-order parameter. The estimates of η, ξ, and χ are based on the linear relationship [45] between the free change density variation $\delta\rho$, deformation potential [46] and/or Vegard strain [47] tensor Ξ_{ij}, and the

TABLE II. Phenomenological parameters of the multiparametric LG model.

Phenomenological parameter in the free	Corresponding dimensionless parameter(s) in the free energy in Eq. (7)	Actual range of dimensionless parameter(s)	Magnitude range of a dimension parameters[a] for a reference materials $SrTiO_3$ and $TiSe_2$
Coupling constant η	η^*	-1.5 to $+1.5$	$\eta = (10^{17} - 10^{19})\cdot$J · m/C^2
Gradient coupling ξ	ξ_S^* and ξ_C^*, which are assumed to be equal	-3 to $+3$	$\xi \cong (10^{-1} - 10^{+1})$J · m^3/C^2
Gradient coupling χ	χ^*	-1 to $+1$	$\chi \cong (10^{-19} - 10^{-17})$ J · m^5/C^2
Gradient coefficients g_C and g_S	Wave vectors $q_C = \sqrt{\frac{g_C}{\alpha_C}}q$ and $k_s = \sqrt{\frac{g_S}{\alpha_S}}k$	Variable	
			$g_S = (10^{-10} - 10^{-11})\cdot$J m^3/C^2
Higher-order gradient coefficients w_C and w_S	w_C^* and w_S^*, which are assumed to be equal	0–10	$w_S \cong (10^{-8} - 10^{-10})$ J · m^{11}/C^2
Higher-order gradient coefficients v_C and v_S	v_C^* and v_S^*, which are assumed to be equal	0–10	$v_S \cong (10^{-27} - 10^{-29})$ J · m^5/C^2
Expansion coefficients $a_C(T) = \alpha_C(\frac{T}{T_C} - 1)$ and $a_S(T) = \alpha_S(\frac{T}{T_S} - 1)$	$\theta_C(T, q_C) = \frac{T}{T_C} - 1 + q_C^2$ and $\theta_S(T, k_S) = \frac{T}{T_S} - 1 + k_S^2$	Functions of temperature and wave vectors; $0.1 \leqslant \frac{T_S}{T_C} \leqslant 10$	$\alpha_S = (10^6 - 10^9)\cdot$J · m/C^2, $T_S = (30{-}400)\cdot$K, $T_C = (0.4{-}200)\cdot$K
Higher-order expansion coefficients b_C and b_S	$\beta_C(q_C) = 1 + w_C^* q_C^2 + v_C^* q_C^4$ and $\beta_S(k_S) = 1 + w_S^* k_S^2 + v_S^* k_S^4$	Functions of wave vectors	$b_S = (10^9 - 10^{12})\cdot$J · m^5/C^4
Energies $f_C = \frac{\alpha_C^2}{b_C}$ and $f_S = \frac{\alpha_S^2}{b_S}$	Ratio $\vartheta = \frac{\alpha_S^2 b_C}{\alpha_C^2 b_S}$	0–10	$f_S \sim (10^5 - 10^7)\cdot$ J/(K^2 · m^3)

[a]Unfortunately, we did not find any reliable data for the values of α_C and b_C (and so for f_C). Because of this, the order parameter ψ_C is selected as dimensionless from the beginning and has an order of unity; its LG parameters α_C and b_C have the same dimension J/m^3. The gradient coefficients g_C, w_C, and v_C have dimensions J/m, J/m, and J · m, respectively. The characteristic gradient scale is $1/q_{CW} \sim 10^{-9}$ m.

elastic stress variation δu_{ij}, whose role is principally important in ferroelastics like $SrTiO_3$ (see, e.g., Ref [12].) and transition-metal dichalcogenides (see, e.g., Refs [3,48]. and refs. therein). Namely, using the relations $\delta u_{ij} \cong \Xi_{ij}\frac{\delta\rho}{e}$ [45] and $\delta\rho = \rho_0 \mathrm{Re}[\psi_C]$ [1] in the biquadratic coupling contribution $W_{ijklmn}u_{ij}u_{kl}P_mP_n$ (also known as nonlinear electrostriction coupling [49,50]), we can estimate that

$$W_{ijklmn}u_{ij}u_{kl}P_mP_n \cong W_{ijklss}\Xi_{ij}^{-1}\Xi_{kl}^{-1}e^2\delta\rho^2P_S^2 \cong W_{ijklss}\Xi_{ij}^{-1}\Xi_{kl}^{-1}\frac{e^2}{\rho_0^2}|\psi_C|^2|\psi_S|^2. \quad \text{(B1a)}$$

Thus,

$$\eta \cong W_{ijklss}\Xi_{ij}^{-1}\Xi_{kl}^{-1}\frac{e^2}{\rho_0^2}. \quad \text{(B1b)}$$

Using the values of parameters $|W_{ijklss}| \sim 10^{11}$ J · m/C^2 [49,50], $\Xi \cong (10^{-29} - 10^{-30})$ m^3 [46,47], $\frac{\rho_0}{e} \cong 10^{26}$ m^{-3}, and $e = 1.6\cdot 10^{-19}$ C, we obtained that $\eta \cong (10^{17} - 10^{19})\cdot$J · m/C^2. The higher-order gradient coupling coefficients ξ and χ are estimated using the characteristic width or uncharged domain walls $d \sim 10^{-9}$ m [12] and wave vector $q_{CW} \sim 10^{+9}$ 1/m [41].

[1] W. L. McMillan, Landau theory of charge-density waves in transition-metal dichalcogenides, Phys. Rev. B **12**, 1187 (1975).

[2] W. L. McMillan, Time-dependent Landau theory of charge-density waves in transition-metal dichalcogenides, Phys. Rev. B **12**, 1197 (1975).

[3] A. N. Morozovska, E. A. Eliseev, H. V. Shevliakova, Y. Yu. Lopatina, G. I. Dovbeshko, M. D. Glinchuk, Y. Kim, and S. V. Kalinin, Correlation between Corrugation-Induced Flexoelectric Polarization and Conductivity of Low-Dimensional Transition Metal Dichalcogenides, Phys. Rev. Appl. **15**, 044051 (2021).

[4] G. Ghiringhelli, M. Le Tacon, M. Minola, S. Blanco-Canosa, C. Mazzoli, N. B. Brookes, G. M. De Luca, A. Frano, D. G. Hawthorn, F. He *et al.*, Long-range incommensurate charge fluctuations in (Y, Nd)$Ba_2Cu_3O_{6+x}$, Science **337**, 821 (2012).

[5] S. Wandel, F. Boschini, E. H. Da Silva Neto, L. Shen, M. X. Na, S. Zohar, Y. Wang, S. B. Welch, M. H. Seaberg, J. D. Koralek *et al.*, Enhanced charge density wave coherence in a light-quenched, high-temperature superconductor, Science **376**, 860 (2022).

[6] Y. Kim, S. J. Kelly, A. Morozovska, E. K. Rahani, E. Strelcov, E. Eliseev, S. Jesse, M. D. Biegalski, N. Balke, N. Benedek *et al.*, Mechanical control of electroresistive switching, Nano Lett. **13**, 4068 (2013).

[7] A. N. Morozovska, E. A. Eliseev, O. V. Varenyk, Y. Kim, E. Strelcov, A. Tselev, N. V. Morozovsky, and S. V. Kalinin, Space charge dynamics in solid electrolytes with steric effect and Vegard stresses: Resistive switching and ferroelectric-like hysteresis of electromechanical response, J. Appl. Phys. **116**, 066808 (2014).

[8] M. Fiebig, T. Lottermoser, D. Frohlich, A. V. Goltsev, and R. V. Pisarev, Observation of coupled magnetic and electric domains, Nature (London) **419**, 818 (2002).

[9] N. A. Spaldin and M. Fiebig, The renaissance of magnetoelectric multiferroics, Science **309**, 391 (2005).

[10] S. Brazovskii and T. Nattermann, Pinning and sliding of driven elastic systems: From domain walls to charge density waves, Adv. Phys. **53**, 177 (2004).

[11] E. A. Eliseev, S. V. Kalinin, Y. Gu, M. D. Glinchuk, V. Khist, A. Borisevich, V. Gopalan, L.-Q. Chen, and A. N. Morozovska, Universal emergence of spatially-modulated structures induced by flexo-antiferrodistortive coupling in multiferroics, Phys. Rev. B **88**, 224105 (2013).

[12] A. N. Morozovska, E. A. Eliseev, M. D. Glinchuk, L.-Q. Chen, and V. Gopalan, Interfacial polarization and pyroelectricity in antiferrodistortive structures induced by a flexoelectric effect and rotostriction, Phys. Rev. B **85**, 094107 (2012).

[13] J.-H. She, J. Zaanen, A. R. Bishop, and A. V. Balatsky, Stability of quantum critical points in the presence of competing orders, Phys. Rev. B **82**, 165128 (2010).

[14] J. C. S. Davis and D. H. Lee, Concepts relating magnetic interactions, intertwined electronic orders, and strongly correlated superconductivity, Proc. Natl Acad. Sci. **110**, 17623 (2013).

[15] E. Fradkin, S. A. Kivelson, and J. M. Tranquada, Colloquium: Theory of intertwined orders in high temperature superconductors, Rev. Mod. Phys. **87**, 457 (2015).

[16] S. D. Edkins, A. Kostin, K. Fujita, A. P. Mackenzie, H. Eisaki, S. Uchida, S. Sachdev, M. J. Lawler, E. A. Kim, J. C. Séamus Davis *et al.*, Magnetic field–induced pair density wave state in the cuprate vortex halo, Science **364**, 976 (2019).

[17] P. Beaud, A. Caviezel, S. O. Mariager, L. Rettig, G. Ingold, C. Dornes, S.-W. Huang, J. A. Johnson, M. Radovic, T. Huber *et al.*, A time-dependent order parameter for ultrafast photoinduced phase transitions, Nat. Mater. **13**, 923 (2014).

[18] M. H. Hamidian, S. D. Edkins, S. H. Joo, A. Kostin, H. Eisaki, S. Uchida, M. J. Lawler, E.-A. Kim, A. P. Mackenzie, K. Fujita *et al.*, Detection of a Cooper-pair density wave in $Bi_2Sr_2CaCu_2O_{8+x}$, Nature (London) **532**, 343 (2016).

[19] L. Nie, A. V. Maharaj, E. Fradkin, and S. A. Kivelson, Vestigial nematicity from spin and/or charge order in the cuprates, Phys. Rev. B **96**, 085142 (2017).

[20] Y. Wang, S. D. Edkins, M. H. Hamidian, J. C. S. Davis, E. Fradkin, and S. A. Kivelson, Pair density waves in superconducting vortex halos, Phys. Rev. B **97**, 174510 (2018).

[21] Y. Yu and S. A. Kivelson, Fragile superconductivity in the presence of weakly disordered charge density waves, Phys. Rev. B **99**, 144513 (2019).

[22] A. Y. Borisevich, E. A. Eliseev, A. N. Morozovska, C.-J. Cheng, J.-Y. Lin, Y. H. Chu, D. Kan, I. Takeuchi, V. Nagarajan, and S. V. Kalinin, Atomic-scale evolution of modulated phases at the ferroelectric–antiferroelectric morphotropic phase boundary controlled by flexoelectric interaction, Nat. Commun. **3**, 775 (2012).

[23] J.-W. Kim, P. Thompson, S. Brown, P. S. Normile, J. A. Schlueter, A. Shkabko, A. Weidenkaff, and P. J. Ryan, Emergent Superstructural Dynamic Order Due to Competing Antiferroelectric and Antiferrodistortive Instabilities in Bulk $EuTiO_3$, Phys. Rev. Lett. **110**, 027201 (2013).

[24] P. B. Littlewood, Chapter 8—Computer simulations of CDW dynamics, Mod. Problems Condens. Matter Sci. **25**, 321 (1989).

[25] N. D. Mathur and P. B. Littlewood, The self-organised phases of manganites, Solid State Commun. **119**, 271 (2001).

[26] A. N. Morozovska, E. A. Eliseev, Y. M. Fomichov, and S. V. Kalinin, Mesoscopic structure of mixed type domain walls in multiaxial ferroelectrics, Phys. Rev. Mater. **4**, 114410 (2020).

[27] A. Biswas, A. N. Morozovska, M. Ziatdinov, E. A. Eliseev, and S. V. Kalinin, Multi-objective Bayesian optimization of ferroelectric materials with interfacial control for memory and energy storage applications, J. Appl. Phys. **130**, 204102 (2021).

[28] A. P. Levanyuk, S. A. Minyukov, and A. Cano, Universal mechanism of discontinuity of commensurate-incommensurate transitions in three-dimensional solids: Strain dependence of soliton self-energy, Phys. Rev. B **66**, 014111 (2002).

[29] M. J. Haun, E. Furman, T. R. Halemane, and L. E. Cross, Thermodynamic theory of the lead zirconate-titanate solid solution system, part IV: Tilting of the oxygen octahedra, Ferroelectrics **99**, 55 (1989); see also M. J. Haun, E. Furman, S. J. Jang, and L. E. Cross, Thermodynamic theory of the lead zirconate-titanate solid solution system, part I: Phenomenology, *ibid.* **99**, 13 (1989).

[30] B. Houchmanzadeh, J. Lajzerowicz, and E. Salje, Order parameter coupling and chirality of domain walls, J. Phys.: Condens. Matter **3**, 5163 (1991).

[31] E. V. Balashova and A. K. Tagantsev, Polarization response of crystals with structural and ferroelectric instabilities, Phys. Rev. B **48**, 9979 (1993).

[32] See Supplemental Materials at http://link.aps.org/supplemental/10.1103/PhysRevB.107.174104 for a mathematical formulation of the problem, description of methods, and auxiliary figures.

[33] E. A. Eliseev, Y. M. Fomichov, S. V. Kalinin, Y. M. Vysochanskii, P. Maksymovich, and A. N. Morozovska, Labyrinthine domains in ferroelectric nanoparticles: Manifestation of a gradient-induced morphological phase transition, Phys. Rev. B **98**, 054101 (2018).

[34] Their order parameter α is related to the complex order parameter $\psi_{CW}(x,t)$, as $\alpha(x,t) = \mathrm{Re}[\psi_{CW}]$. Using their assumption, $\psi_{CW} = A_{CW}\exp(-i\mathbf{Qr})$, where A_{CW} is a slow-varying complex amplitude, we obtained that $\nabla\psi_{CW} = \exp(i\mathbf{Qr})(\nabla A_{CW} - i\mathbf{Q})$. Thus, their expression for the gradient term may originate from $|\vec{e}_Q\nabla\psi_{CW}|^2 \cong \frac{1}{Q^2}|\mathbf{Q}\cdot(\nabla A_{CW} - i\mathbf{Q})|^2$, where the unit vector $\vec{e}_Q = \frac{1}{Q}\mathbf{Q}$ is introduced.

[35] L. D. Landau and I. M. Khalatnikov, On the anomalous absorption of sound near a second order phase transition point, Dokl. Akad. Nauk SSSR **96**, 496 (1954).

[36] J.-J. Wang, B. Wang, and L.-Q. Chen, Understanding, predicting, and designing ferroelectric domain structures and switching guided by the phase-field method, Ann. Rev. Mater. Res. **49**, 127 (2019).

[37] https://www.wolfram.com/mathematica.

[38] Y. Zhang, H. X. Yang, C. Ma, H. F. Tian, and J. Q. Li, Charge-Stripe Order in the Electronic Ferroelectric $LuFe_2O_4$, Phys. Rev. Lett. **98**, 247602 (2007).

[39] A. Bussmann-Holder and H. Bottner, Charge-density-wave formation in $TiSe_2$ driven by an incipient antiferroelectric instability, J. Phys.: Condens. Matter **14**, 7973 (2002).

[40] Tae-Ho Park, O. P. Uzoh, and Han-Yong Choi, Maximal superconductivity in proximity to the charge density wave quantum critical point in Cu_xTiSe_2, Phys. Rev. B **104**, 184506 (2021).

[41] A. Kogar, A. Zong, P. E. Dolgirev, X. Shen, J. Straquadine, Y.-Q. Bie, X. Wang, T. Rohwer, I-C. Tung, Y. Yang *et al.*, Light-induced charge density wave in $LaTe_3$, Nat. Phys. **16**, 159 (2020).

[42] R. Russell, N. Ratcliff, K. Ahadi, L. Y. Dong, S. Stemmer, and J. W. Harter, Ferroelectric enhancement of superconductivity in compressively strained $SrTiO_3$ films, Phys. Rev. Mater. **3**, 091401(R) (2019).

[43] C. Herrera, J. Cerbin, A. Jayakody, K. Dunnett, A. V. Balatsky, and I. Sochnikov, Strain-engineered interaction of quantum polar and superconducting phases, Phys. Rev. Mater. **3**, 124801 (2019).

[44] M. M. Alyörük, Y. Aierken, D. Çakır, F. M. Peeters, and C. Sevik, Promising piezoelectric performance of single layer transition-metal dichalcogenides and dioxides, J. Phys. Chem. C **119**, 23231 (2015).

[45] A. N. Morozovska, E. A. Eliseev, A. K. Tagantsev, S. L. Bravina, L.-Q. Chen, and S. V. Kalinin, Thermodynamics of electromechanically coupled mixed ionic-electronic conductors: Deformation potential, Vegard strains, and flexoelectric effect, Phys. Rev. B **83**, 195313 (2011).

[46] H. F. Tian, J. R. Sun, H. B. Lü, K. J. Jin, H. X. Yang, H. C. Yu, and J. Q. Li, Electrostatic potential in manganite-based heterojunctions by electron holography, Appl. Phys. Lett. **87**, 164102 (2005).

[47] D. A. Freedman, D. Roundy, and T. A. Arias, Elastic effects of vacancies in strontium titanate: Short-and long-range strain fields, elastic dipole tensors, and chemical strain, Phys. Rev. B **80**, 064108 (2009).

[48] A. N. Morozovska, E. A. Eliseev, G. I. Dovbeshko, M. D. Glinchuk, Y. Kim, and S. V. Kalinin, Flexo-induced ferroelectricity in low dimensional transition metal dichalcogenides, Phys. Rev. B **102**, 075417 (2020).

[49] N. A. Pertsev, A. K. Tagantsev, and N. Setter, Phase transitions and strain-induced ferroelectricity in $SrTiO_3$ epitaxial thin films, Phys. Rev. B **61**, R825 (2000).

[50] A. Kvasov and A. K. Tagantsev, Role of high-order electromechanical coupling terms in thermodynamics of ferroelectric thin films, Phys. Rev. B **87**, 184101 (2013).